Four Equation k-omega Based Turbulence Model with Algebraic Flux for Supercritical Flows

Timothy P. Grunloh*
Illinois Rocstar LLC
108 Hessel Blvd
Champaign, IL 61820
www.illinoisrocstar.com
*tpgrunloh@illinoisrocstar.com

Abstract
Hydrocarbon and nuclear fuels will contribute substantially to the growing global energy portfolio for some time to come. At the same time atmospheric carbon levels and economic concerns are increasingly shaping the power generation environment. Supercritical fluid technologies are being investigated to address both concerns. For example, direct fired supercritical CO_2 power cycles offer key advantages for carbon capture and thermal efficiency. Additionally, the supercritical water reactor Generation IV nuclear reactor allows higher power densities and more efficient operation than current pressurized or boiling water reactors. As these technologies are developed, a need exists for accurate, yet cost-effective modeling and simulation solutions to assist with design and safety calculations. Supercritical fluid properties are strongly dependent on temperature which results in a number of unique flow features. Among these features are the complex buoyancy and buoyancy-turbulence interaction behaviors exhibited by supercritical flows that are not found in liquid or gas flows. Therefore, standard turbulence models with current model coefficient values are not likely to be applicable to supercritical fluid flows.

The subject of this paper is efficient modeling and simulation of supercritical flows to support nascent technologies growing to maturation and operational deployment. We present a framework for developing Reynolds-Averaged Navier Stokes turbulence models specifically equipped for the challenges of supercritical flows. A novel formulation of the algebraic heat flux model of the buoyancy production of turbulence term is used with a traditional shear stress transport model. To produce a new turbulence model for supercritical channel flows, the empirical coefficients of the resulting four equation model were calculated from data previously published by other authors regarding upward supercritical flow through heated pipes. The presented SST k_t-ω_t approach was validated against heated tube experiments to show predictive capabilities in moderate flow conditions, where buoyancy effects are important but not dominating of inertial effects.

Keywords: RANS turbulence models; supercritical flow; algebraic flux, buoyancy production of turbulence

1 Introduction

As energy appetites around the world continue to grow, cost-effective and safe energy cycles will continue to be in constant demand [1]. Using supercritical carbon dioxide (sCO_2) or water (sH_2O) as a working fluid in power cycles enables operation at higher efficiency because no phase change occurs in the supercritical regime and latent heat of evaporation is not a factor. The fluid also facilitates higher operating temperatures, improving Carnot efficiency. Direct capture of combustion-produced carbon for fossil fueled plants is a highly beneficial characteristic in an economic environment characterized by increasing concern about atmospheric carbon levels. As a result, supercritical fluids are increasingly being evaluated for adoption into a variety of power cycles including both fossil fuel and nuclear [2]. The Supercritical Water Reactor (SCWR), for example, has been identified by the GenIV International Forum as a leading candidate for future power reactors [3].

The applications of turbulence models developed for supercritical flows are potentially wide ranging. For example, the United States Department of Energy (DOE) identified several components of direct-fired fossil fuel cycles which are specifically in need of additional research and development. Among them are pressurized oxy-combustion and sub-critical CO_2 pumping and compression [4]. Combustion within the working fluid generates strong temperature and density gradients leading to a number of phenomena including strongly enhanced turbulent mixing and potentially strong buoyancy effects. Control of turbomachinery is difficult near the critical point and accurate models are required for pump design. Thermal transport in heat exchangers leads to strong near-wall temperature gradients and buoyancy effects. In nuclear reactors, the heating along fuel rods will interact with supercritical fluid density through both thermal hydraulic and neutronic paths. Therefore, developing models which are capable of resolving physics unique to supercritical flows is an important task as these advanced power cycles are designed and deployed.

As sCO_2 and sH_2O cycles are designed, evaluated, and deployed, modeling and simulation (M&S) activities are carried out alongside experimental studies to support safe, economically optimized design and operation. Among existing computational approaches to turbulence, only Direct Numerical Simulation (DNS) methods fully resolve turbulent effects but are prohibitively expensive for most cases. Large Eddy Simulation (LES) resolves some scales of turbulence and provides extremely accurate solutions for many shear-dominated flows. While the cost of a single simulation has become quite tractable [5], LES is too expensive to be useful for applications such as design and optimization which require many simulations, often ranging from 10 to 10^6 or more. This method is ideally suited for understanding detailed flow mechanisms, such as thermal striping when hot and cold streams mix. Reynolds-Averaged Navier-Stokes (RANS) turbulence models are ideal for design and optimization applications that require large numbers of simulations and for which resolving all aspects of the flow field is not a requirement. However, RANS models are not universally applicable. The present work is therefore intended to contribute to developing RANS turbulence models specifically for supercritical flows.

Developing RANS models for these flows requires a detailed understanding of key physics. Due to the sensitive variation of thermophysical properties with temperature, supercritical fluids exhibit complex behavior. For example, consider flow of supercritical fluid through a heated channel in a gravitational field, a problem well supported by a wealth of published data [6]. For upward flow, the buoyancy production term plays a key role in heat transfer deterioration arising from laminarization. Heat transfer deterioration results from low density fluid collecting near a heated wall causing abrupt decrease in near-wall heat capacity of the fluid, somewhat analogous to departure from nucleate boiling. Bae et al. [7] showed through DNS that any increase in wall temperature following heat transfer deterioration is limited by axial profile flattening with accompanying decreased shear stress production. This can lead to a change in sign of buoyant forces, which can dominate shear stress effects in the boundary layer. Bae et al. [7] also found that, in downward flows, the buoyancy effect increases the turbulence level, which enhances heat transfer. Standard models have been found generally unable to simulate these phenomena [8]. A more sophisticated algebraic flux model approach has been investigated by a number of authors over the past several decades [9–14]. In general, the simulation of highly buoyant flows, such as those expected with supercritical fluids, is a particularly active field of inquiry [15–17]. Researchers at the University of Pisa have in particular undertaken significant efforts towards understanding the nature of heat transfer in supercritical fluids [18–27]. They found that standard turbulence modeling approaches are unable to capture supercritical heat transfer phenomena such as enhanced or deteriorated heat transfer. For example k-ε models were found to overestimate heat transfer deterioration while k-ω underestimated the phenomenon. Pucciarelli et al. [24] found that algebraic flux modeling (AFM) approaches to buoyancy production formulation produced substantially improved results over traditional approaches such as simple and generalized gradient diffusion hypotheses.

In this paper, we apply AFM for the buoyancy production term in simulating upward flows of heated supercritical fluids. This physical configuration was chosen for the wealth of existing data and for the complex physical phenomena arising from strong buoyant forces. Because the present approach requires the solution of additional transport equations alongside the standard two equation turbulence models, the generated models are referred to as four equation models. To the knowledge of the authors, the formulation of the additional transport equations used here is novel. Relevant publications typically use a k_t-ε_t formulation analogous to the k-ε turbulence model [14,24,28], while we employ a k_t-ω_t formulation analogous to the k-ω turbulence model. This formulation was chosen to leverage the superior near-wall performance of the k-ω model. Models were tested in two regimes based on flow rates. Models performed better when applied to similar conditions as those from which experimental data were gathered. For example, data from experiments with low flow rates produced models more applicable to other cases with low flow rates. The algebraic flux model was important for both low and moderate flow cases, but was critical for the former flow regime.

2 Modeling Approach

2.1 Background

This section describes the modeling framework used in this work. The system pressure was assumed constant and temperature dependent thermophysical properties were assembled from NIST data into lookup tables [30]. The turbulence model was developed from careful consideration of the physics observed from previous work and from published experimental studies. One such study, performed by Kim and Kim [29], is summarized in Fig. 1. This figure shows experimentally measured wall temperatures along the heated

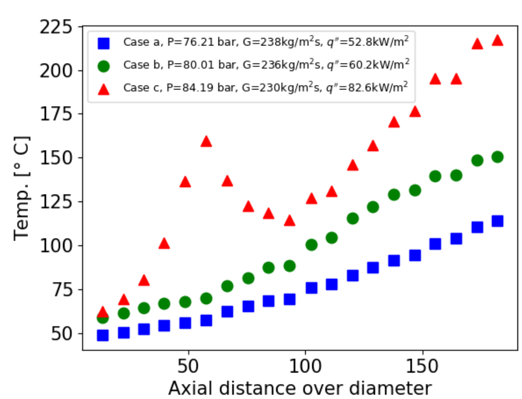

Figure 1: Data collected by Kim and Kim[29] of sCO_2 flow through heated channel. Under some conditions heat transfer deterioration leads to temperature peaking along the channel length.

section of upward sCO_2 flow for several cases differentiated by system pressure, flow rate, and applied heat flux. As is clear from the figure, the qualitative and quantitative behavior of the heat transfer can be exceedingly sensitive to the flow conditions. Case c featured the lowest flow rate and highest heat flux of the set. Consequently, these data exhibit interesting behavior in the form of a striking temperature peak within the heated section, a phenomenon also observed in the DNS simulations of Bae et al. [7].

Zhang et al. [14] performed compelling analyses motivating the use of AFM for buoyancy production of turbulence including experimental measurements of wall temperatures along heated channels of supercritical water. They additionally simulated the experiment to assess various turbulence models' ability to capture supercritical flow physics. Consider Fig. 2 as a summary of their results. In this case, the Shear Stress Transport (SST) model strongly overpredicted wall temperatures. However, the Zhang formulation of AFM (using k-ε turbulence and k_t-ε_t AFM) quite accurately captured the experimental data qualitatively and quantitatively.

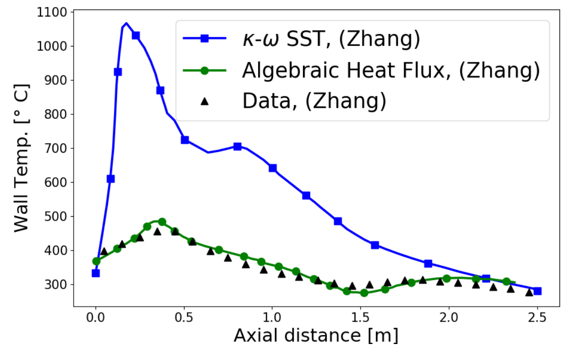

Figure 2: Summary of analysis by Zhang[14] showing simulation of supercritical water flow through heated channel. Standard shear stress transport models are not equipped to model supercritical heat transfer.

2.2 Turbulence Model

The specific model used in this paper uses SST for Reynolds stress closure and a k_t-ω_t AFM formulation for the buoyancy production term. The SST model combines the k-ω and k-ε turbulence models such that the models behave like k-ω in the boundary layer and k-ε in the interior, free shear flow region [31]. Over recent years, this model has gained traction and is a major model supported by many CFD packages. A k-ω-based approach to AFM was chosen for ease-of-implementation as compared to an SST-based approach, which may be a subject for future work.

While a combination of standard k-ω and k-ε models, the SST approach used in this paper solves transport equations for k and ω which are interpreted as turbulence kinetic energy and turbulence frequency, just as in the k-ω model. The SST transport equations are more complicated, however, and include a number of auxiliary relations. Precise formulations of these equations and relations are well-documnted in the literature. The SST model implemented in *OpenFOAM* v4.1, used for this work, was based on the description provided by Menter and Esch [32] with updated coefficients [33] and an optional term for rough walls adapted from Hellsten [34]. The k_t-ω_t AFM formulation used in this work is discussed in the following section.

2.3 Buoyancy Production of Turbulence

The influence of buoyancy on turbulence in supercritical flows has been analyzed by, among others, Zhang and colleagues [14]. In the scientific literature three primary methods are commonly employed for addressing these effects. One of the original approaches is the simple gradient diffusion hypothesis (SGDH):

$$\overline{u_i' T'} = -\frac{\nu_t}{Pr_t}\frac{\partial \overline{T}}{\partial x_i}, \tag{1}$$

where Pr_t is the turbulent Prandtl number. A more advanced approach is the generalized gradient diffusion hypothesis (GGDH):

$$\overline{u_i' T'} = -C_t \frac{k}{\epsilon}\overline{u_i' u_j'}\frac{\partial \overline{T}}{\partial x_j}, \tag{2}$$

where C_t is a model coefficient. One of the most sophisticated approaches is the algebraic flux model (AFM):

$$\overline{u_i' T'} = \frac{-\overline{u_i' u_j'}\frac{\partial \overline{T}}{\partial x_j} - (1 - C_{t2})\,\overline{u_j' T'}\frac{\partial \overline{u}_i}{\partial x_j} - (1 - C_{t3})\,\beta g_i \overline{T'^2}}{C_{t1}\frac{\epsilon}{k}}, \tag{3}$$

where C_{t1}, C_{t2}, and C_{t3} are model coefficients. These approaches are discussed in depth in the scientific literature (see [14] for example). SGDH is generally understood to be inapplicable for any complex flows. GGDH is an improvement over SGDH, but still struggles with some complex flows. The AFM approach is therefore used in this work.

The AFM requires knowledge of $\overline{T'^2}$, also referred to as k_t. Among others Pucciarelli et al. address this by solving additional transport equations analogous to those used for k and ε [24]. While the majority of AFM implementations found in the literature use a k_t-ε_t formulation, we employed a k_t-ω_t formulation. We hypothesized that the superior near wall behavior associated with k-ω formulations would translate to improved behavior of the AFM implementation. The k_t-ω_t AFM transport equations were implemented by adding the transport equations of Eq. 4 and Eq. 5 to existing turbulence models:

$$\frac{\partial \rho \omega_t}{\partial t} + \overline{u}\cdot\nabla(\rho\omega_t) - \nabla\cdot\left[\rho\left(\alpha_{\omega_t}\nu_T + \nu\right)\nabla\omega_t\right] = \rho\gamma_t G_t \frac{\omega_t}{k_t} - \frac{2}{3}\rho\gamma_t \nabla\cdot\overline{u}\omega_t - \beta_t \rho \omega_t^2, \tag{4}$$

$$\frac{\partial \rho k_t}{\partial t} + \overline{u}\cdot\nabla(\rho k_t) - \nabla\cdot\left[\rho\left(\alpha_{k_t}\nu_T + \nu\right)\nabla\omega_t\right] = \rho G_t - \frac{2}{3}\rho\nabla\cdot\overline{u}\omega_t - C_{\mu_t}\rho\omega_t k_t, \tag{5}$$

where G_t is given by:

$$G_t = \overline{u_i' T'}\frac{\partial \overline{T}}{\partial x_i}. \tag{6}$$

In the employed algorithm, the k_t-ω_t equations are solved just prior to the k-ω equations of the SST model. Adding these transport equations enables calculation of $\overline{T'^2} = k_t$ allowing calculation of the $\overline{u_j' T'}$ correlation as defined by Eq. 7, which includes a term proportional to the turbulence anisotropy tensor, a_{ij}, for completeness:

$$\overline{u_j' T'} = -C_t \tau\left[C_{t1}\overline{u_i' u_j'}\frac{\partial \overline{T}}{\partial x_i} + (1 - C_{t2})\,\overline{u_i' T'}\frac{\partial \overline{u}_j}{\partial x_i} + (1 - C_{t3})\,\beta g_j \overline{T'^2}\right] + c_{t1}' a_{ij}\overline{u_i' T'}, \tag{7}$$

where β is given by

$$\beta = -\frac{1}{\rho}\frac{\partial \rho}{\partial \overline{T}}, \tag{8}$$

and the turbulence anisotropy tensor is given by

$$a_{ij} = \frac{\overline{u_i' u_j'}}{k} - \frac{2}{3}\delta_{ij}. \tag{9}$$

Eq. 7 is implicitly defined for $\overline{u_j' T'}$. An explicit expression can be easily defined by defining several intermediate variables:

$$v_j = \overline{u_j' T'}, w_j = C_{t1}\overline{u_i' u_j'}\frac{\partial \overline{T}}{\partial x_i}, x_{ij} = (1 - C_{t2})\frac{\partial \overline{u}_j}{\partial x_i}, y_j = (1 - C_{t3})\,\beta g_j \overline{t'^2}, z_{ij} = c_{t1}' a_{ij}. \tag{10}$$

Using these variables, the implicit equation for $v_j = \overline{u_j' T'}$ is rewritten as follows

$$v_i = -C_t \tau \left[w_i + x_{ij} v_j + y_i\right] + z_{ij} v_j, \tag{11}$$

which leads directly to

$$v_i = -C_t \tau \left[\delta_{ij} + C_t \tau x_{ij} - z_{ij}\right]^{-1}\left[w_j + y_j\right], \tag{12}$$

where δ_{ij} is the identity matrix. This expression is then directly used to calculate $v_j = \overline{u_j' T'}$. Due to the formulation of thermophysical models in *OpenFOAM* it is easier to gain access to the fluid density variable. Therefore Eq. 13 is used to relate temperature gradients to density gradients.

$$\frac{\partial \overline{T}}{\partial x_j} = \frac{\partial \rho}{\partial x_j}\frac{\partial \overline{T}}{\partial \rho} = -\frac{1}{\rho\beta}\frac{\partial \rho}{\partial x_j} \tag{13}$$

Once calculated, $\overline{u_j' T'}$ actually affects the flow through source terms to the k and ω transport equations of the SST turbulence model (not to be confused with the k_t-ω_t equations of Eqs. 4 and 5) discussed in Section 2.2:

$$S_k = C_g \rho \beta g_j \overline{u_j' T'}, \tag{14}$$

$$S_\omega = C_g \rho \beta g_j \overline{u_j' T'}\frac{\omega}{k}, \tag{15}$$

where C_g was used as a fitting convenience and is taken to be unity in the results reported here. Some published values for the AFM coefficients are given in Table 1.

Because stability and convergence are issues pervasive in CFD, the numerical parameters used in *OpenFOAM* v4.1 are discussed briefly. The standard SIMPLE solver with buoyancy was used to solve the system [35]. We used the van Leer discretization scheme [36] for the velocity, pure upwind for k_t and ω_t, and limited linear discretizations for k and ω equations. Convergence was assumed when the enthalpy residual passed below 10^{-6}. Under-relaxation factors of 0.5 were used for all equations except for enthalpy, which was 0.6, and k_t-ω_t, which were 0.4. Steady state was assumed for all calculations.

Table 1: Selected AFM coefficients from literature.

Model	C_t	C_{t1}	C_{t2}	C_{t3}	c'_{t1}
Kenjereš [13]	0.15	0.6	0.4	0.4	1.5
Zhang [14]	0.66	1	0.33	0.33	0

2.4 Boundary Conditions

Wall treatment of AFM transport equations for k_t and ω_t was adapted in analogy from standard treatment for k and ω. The no slip boundary for ω_t was therefore accomplished with Eq. 16.

$$\omega_{t,wall} = \sqrt{\left(\frac{6\nu}{\beta_1 y^2}\right)^2 + \frac{k_t}{\sqrt{C_\mu \kappa^2 y^2}}}, \tag{16}$$

where ν is the kinematic viscosity, y is the wall distance, $\beta_1 = 0.075$, $C_\mu = 0.09$, and $\kappa = 0.41$.

No slip for the k_t variable was realized with a zero gradient condition, similar to the low Reynolds number approximation for turbulent kinetic energy. This approach is analogous to that taken by Zhang et al. [14] who used Eq. 17 as a boundary for ε_t:

$$\varepsilon_{t,wall} = \alpha \left(\frac{\partial \sqrt{k_t}}{\partial y}\right)^2 \tag{17}$$

3 Results

In Section 2, the turbulence models used and developed for the efforts described in this paper were described theoretically. In this section, we tailor the models to realistic simulations and compare the results to previously published experimental data. Details of the *OpenFOAM* CFD model are discussed in Section 3.1. Section 3.2 discusses the approach taken to develop the models, with the produced models presented in Section 3.3. Broadly speaking, the approach uses experimental data from supercritical flows to inform model formulations. By developing models from these data, we seek to create RANS models that are uniquely suited to capture the complex physical phenomena characteristic of supercritical fluids.

3.1 CFD Model

The simulations presented in this paper were carried out with the "buoyantSimpleFoam" solver in *OpenFOAM* v4.1. Meshes were generated, primarily with *OpenFOAM* utilities and some help from the open source tool *SALOME*, by first creating a tetrahedral base mesh which was converted into a polyhedral mesh. Near-wall prismatic layers were then added. Finally the axial length of the mesh was created by extruding layers of the radial mesh to create the final pipe. Extruding meshes allows for higher cell density in the radial direction where flow gradients are steeper. The type of problem addressed in this paper is shown schematically in Fig. 3a. Supercritical fluid enters a circular pipe from the bottom and flows upward through a section to which a heat flux is applied. In this study, the wall temperature T_{wall}, is used as a key performance metric.

The problems simulated in this work include conditions which induce heat transfer deterioration (HTD) demonstrated by the local temperature peak a short distance downstream of the inlet of the heated section in Fig. 3a. This phenomenon has been discussed by several authors [14, 24]. HTD is a key factor in buoyant supercritical flows and test cases were specifically chosen to include it. HTD can be thought of as analogous to departure from nucleate boiling (DNB) where near-wall boiling becomes so intense that a gas film forms and greatly diminishes heat transport. In HTD, heat addition to the supercritical flow causes a substantial decrease in density. When flow is slow, less low density fluid is removed from the near wall region and continued heat addition results in marked localized degradation of heat removal capacity. Similar to DNB, HTD results in hot spots which may cause material melting and failure, potentially leading to unsafe operating states. HTD can be reduced by ensuring sufficient flow rate and limiting heat fluxes. Accurate modeling is required to efficiently deploy mitigation without unduly affecting the economics of a power cycle.

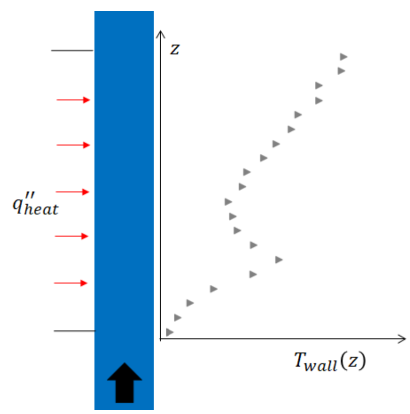

(a) Schematic diagram showing configuration of upward flow problems simulated in this work. Grey triangles represent wall temperature values along the heated section.

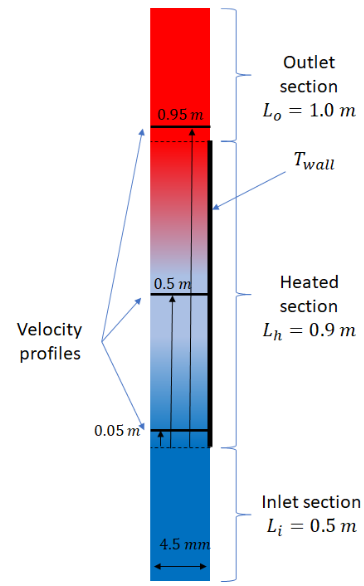

(b) Diagram of computational setup showing key length scales and indicating locations of considered results.

Figure 3: Upward supercritical flow simulated with *OpenFOAM*.

The computational domain was broken into 3 sections, as shown in Fig. 3b. An inlet length of 0.5 m precedes a heated section of 0.9 m which is the region of interest. Finally an outlet section of 1.0 m is downstream of the heated section. The inlet and outlet sections are used to separate in/outflow boundary conditions, which may introduce unphysical effects, from the important domain sections. We found the outlet length to be especially important with shorter lengths potentially leading to substantial instabilities. The most relevant results extracted from the simulation are the wall temperatures. As shown in the figure, these data are taken from a line along the wall of the heated section. We also examine several radial velocity profiles taken, relative to the heated section, just downstream of the entrance, near the middle, and just downstream of the exit.

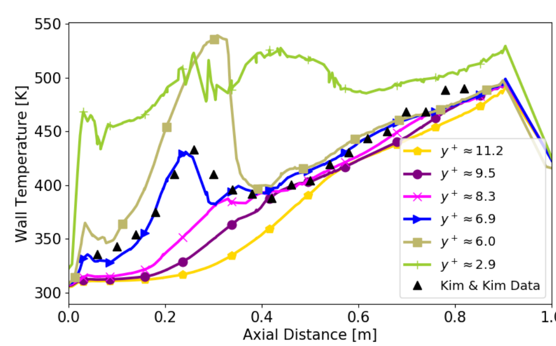

Figure 4: Sensitivity of wall temperature profile to y^+ with AFMSST.lf.3 turbulence model. Results compared to data from Kim and Kim [29].

In order to ensure that the mesh used for this study did not have undue influence over the simulation, a mesh sensitivity study was carried out on a complex problem with results shown in Fig. 5. First, the axial discretization was tested by multiplying the number of axial layers in the base mesh by 0.5 and 2.0. As can be seen in Fig. 5a the wall temperature solution is not strongly affected by changes in the axial mesh density. In this case the near-wall and radial mesh parameters were held constant. Secondly, the effects of radial mesh density were testing by holding near-wall and axial mesh parameters constant with results shown in Fig. 5b. Over a fairly wide range of internal cell density, the results of the simulation do not change substantially.

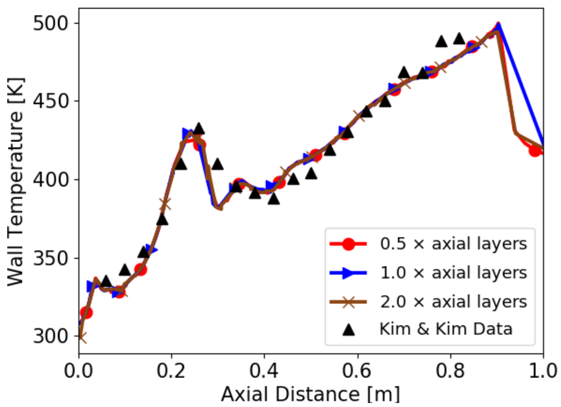

(a) Effects of varying the number of axial layers. Near wall mesh and internal polyhedral mesh kept constant.

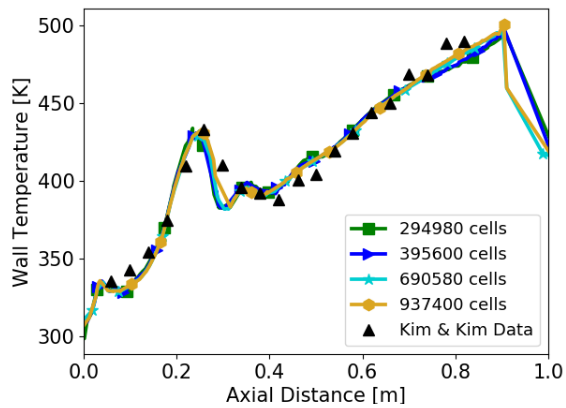

(b) Effects of varying internal polyhedral cell density. Wall mesh and axial layers kept constant.

Figure 5: Mesh sensitivity study using "lowFlow" case with AFMSST.lf.3 turbulence model. Results compared to data from Kim and Kim [29].

Near wall effects were explored with the results shown in Fig. 4. Unlike the previous figures, the wall temperature here shows significant dependence on the dimensionless distance wall distance, y^+. At higher values of y^+, the temperature peak is not resolved, while lower values of y^+ lead to a much larger peak. At the lowest y^+ value tested, a high wall temperature is observed throughout the heated section and the temperature peak is not visible. Several factors may influence this behavior. The high wall temperatures at low y^+ were observed throughout this project and are suspected to result from wall functions performing poorly very near the wall. This is a known issue, which has been addressed in the more recent *OpenFOAM* v5.0 or v6.0 which includes updated wall functions designed to improve low Re wall behavior for ε and ω [37]. Because finite volume methods define most field values at cell centers, calculating edge values requires interpolation. Temperature gradients are steep near the wall and small errors in calculations can lead to large differences in wall temperature results, especially when using higher y^+ meshes. Finally, the developed model may simply depend on y^+, especially in the $6 < y^+ < 12$ region discussed here which is known to be challenging for wall functions. The flow rates studied limited our ability to reach $y^+ > 30$, a more preferable region for wall-modeled simulations.

The authors believe the combination of poor low Re performance for ω and dependence of the model on y^+ to be the primary causes. Upgrading to the improved wall functions of *OpenFOAM* v5.0 or higher will enable this model to be used with much lower y^+ meshes. Resolving the turbulent boundary layer will then reduce the model's dependence on near wall mesh. One can conclude from these results that near-wall behavior is critical to fully capture the heat transfer effects of buoyant supercritical flow. The wall-modeled mesh used in this case featured 3 prism layers near the edge as the turbulent boundary layer is primarily modeled. The coarse mesh is 395,600 cells in total with an average of ≈ 7.12 faces per cell. This total includes 154,800 hexahedra and 240,800 polyhedra.

3.2 Coefficient Optimization

Turbulence models generally contain a number of semi-empirical or empirical coefficients. Common models such as k-ε or k-ω are often considered alongside standard sets of coefficients which are generated by comparing model results against sets of canonical flow problems. Because this set of problems is finite, the traditionally quoted sets of model coefficients cannot be applied to every possible flow with an expectation of high quality results. Therefore, a key aspect of developing for-purpose turbulence models involves calculating optimized sets of model coefficients.

As discussed by Duffey and Pioro [6], a wide variety of studies on supercritical flow through heated channels have been reported in the literature over the past few decades. The model development effort discussed had the objective of simulating an experiment performed by Kim and Kim [29], chosen because the experiments were straightforward to explore, yet included complex phenomena. Two cases were selected from Kim and Kim's study (key parameters are listed in Table 2, both for upward flows) to guide the turbulence modeling work. The "lowFlow"case is characterized by a low flow rate such that buoyancy effects are expected to play a substantial role. A more moderate flow rate case is referred to as "modFlow". Buoyant effects are expected to play a less critical role in this scenario. Considering both cases enables us to analyze multiple physical mechanisms and to chart a path forward for developing RANS models capable of simulating wide ranges of supercritical fluid flows.

Table 2: Chosen test case parameters from Kim and Kim [29].

Case	Inlet Velocity [m/s]	Pressure [MPa]	Heat Flux [kW/m^2]	Fluid
lowFlow	0.31	8.194	82.6	CO_2
modFlow	0.67	8.419	103.1	CO_2

Data from these experiments were used to obtain sets of model coefficients by simulating them and comparing the calculated wall temperatures to those measured. The coefficients were optimized with a trust region reflexive nonlinear least squares method [38] implemented in the *SciPy* Python library [39]. The *OpenFOAM* simulation was wrapped in Python code which took model coefficients as input and output the linear difference between measured and calculated temperature. The optimization algorithm sought to minimize this difference by estimating a Jacobian with which the input parameter space can be efficiently explored. Of course, this method is not guaranteed to converge to the most optimum set of coefficients when local extrema are present. Therefore, the results were frequently inspected and changes to starting parameter sets were used to guide the algorithm towards global extrema. The *SciPy* algorithm is capable of incorporating uncertainty in input data as well as outputting fitting optimality measure. In future work, these features will be used to further improve fitting quality.

3.3 Model Development

The models we created are further discussed in Section 3.3.1 in the context of the Kim and Kim data used to generate them. In Section 3.3.2, the models are used to compute the Kim and Kim scenarios that they were not developed from (i.e., a model tuned from "lowFlow" data is used to simulate the "modFlow" case). We refer to this as "testing" rather than validation because the data are part of the same experiment and are subject to common cause faults. Lastly, an additional model referred to as AFMSST.lfmf.1 was developed using both sets of data. In the sections to follow, we present results in terms of wall temperature along a heated section of upward axial flow. Note that all experimental data were captured from thermocouple measurements. An axial distance of 0 represents the entrance of the heated section and larger axial distances represent higher elevations (see Fig. 3b).

3.3.1 Model Tuning

Fig. 6 shows the results of model coefficient fitting for sCO_2 turbulence models based on the SST model. With the exception of the default SST (SST.d) curve, all plots were calculated with coefficients calculated from fitting the experimental data from Kim and Kim [29]. The specific data used from the "lowFlow" case of Table 2 are also plotted in Fig. 6. The SST.d poorly represents the data, both qualitatively and quantitatively. The SST model with optimized coefficients (SST.lf) is significantly better at representing the curve. The left edge of the internal temperature peak is particularly well predicted while the right edge is less well represented. The remainder of the curve provides a reasonable, qualitative reproduction of the overall trend of the data.

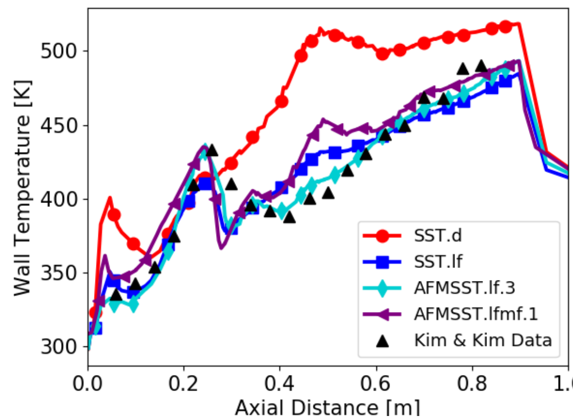

Figure 6: Comparison of SST-based models from the "lowFlow" case. SST.d is default *OpenFOAM* model. SST.lf, AFMSST.lf.3, and AFMSST.lfmf.1 are models developed by Illinois Rocstar. Data from Kim and Kim [29].

We added the algebraic flux model to the standard SST model and generated several sets of coefficients. The AFMSST.lf.3 curve shows the best representation of the experimental data. The left edge of the internal temperature peak is well resolved and the local maximum is also quite well reproduced. The right edge of the internal peak is somewhat poorly predicted once again. The remainder of the experimental data are well represented, both qualitatively and quantitatively. The AFMSST.lfmf.1 model, tuned from both sets of data, matches the internal temperature peak very well. However, this model shows another peak around the axial distance of 0.5 that is likely an artifact from the "modFlow" case.

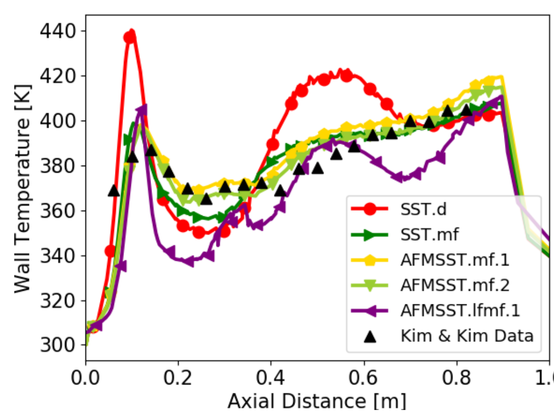

Figure 7: Comparison of SST-based models for "modFlow" case. SST.d is default *OpenFOAM* model. SST.mf, AFMSST.mf.1, AFMSST.mf.2, and AFMSST.lfmf.1 are models developed by Illinois Rocstar. Data from Kim and Kim [29].

This analysis as well as those that follows highlights the need for turbulence models to be properly calibrated for the physics to be modeled. In this case the "out-of-the-box" SST coefficients (SST.d) lead to a qualitatively and quantitatively poor estimate of the wall temperatures. However, some tuning led the SST.lf model to much better approximate the solution. Even further improvement was found by adding physics to the models through additional terms in the AFMSST models. In general, all turbulence models (especially RANS) are semi-empirical and the coefficients include contributions from physics which are not explicitly modeled. Therefore, implicit assumptions about physical mechanisms and their relative strengths are made through selection of model coefficients. Of course, these "implicit physics" will vary from case to case, highlighting the motivating factor for this work: to take steps to determine the best physics models and coefficients steps for thermal supercritical flows.

All coefficients are given in Table 3, which shows the coefficients for the k_t and ω_t transport equations and Table 4, which shows the coefficients from the SST portion of the AFM model (i.e., k and ω transport equations). It should be noted that these results do not provide information about the predictive capability of the models since they are being compared to data to which they are fit. However, the figures do provide information about which models are able to actually resolve the physics of the model. These results suggest that the addition of AFM to the SST model improves our ability to resolve heated supercritical fluid behaviors. We should also note that some of the AFMSST models substantially alter the base SST coefficients (Table 4). Therefore, these models may perform poorly in regions of the flow far away from high thermal gradients or the critical point. While these models are intended to be specifically adapted to thermal supercritical flows and not to replace SST models for all purposes, future work should include evaluating how these models work in non-channel flows that may include approximately isothermal regions.

Table 3: AFM coefficients for RANS models developed for supercritical flows.

Model	C_t	C_{t1}	C_{t2}	C_{t3}	c'_{t1}	β_c	β_t	C_{μ_t}	γ_t	α_{k_t}	α_{ω_t}
AFMSST.lf.3	1.0	0.95	1.31	1.58	2.03	1.0	0.072	.09	0.52	0.5	0.5
AFMSST.mf.1	1.0	0.503	1.9	2	1.2	1.0	0.072	.09	0.52	0.5	0.5
AFMSST.mf.2	1.0	0.64	1.88	1.44	1.24	1.0	0.072	.09	0.52	0.5	0.5
AFMSST.lfmf.1	1.0	1.12	1.87	1.46	0.83	1.0	0.072	0.09	0.52	0.56	0.6

These coefficients were used in conjunction with the corresponding coefficients in Table 4

Table 4: SST Coefficients coefficients for RANS models developed for supercritical flows.

Model	α_{k1}	α_{k2}	$\alpha_{\omega 1}$	$\alpha_{\omega 2}$	γ_1	γ_2	β_1	β_2	a_1	b_1	c_1
SST.d	0.85	1.0	0.5	0.856	γ_d	0.44	0.075	0.0828	0.31	1.0	10
SST.lf	0.43	1.47	0.72	0.16	0.82	1.11	0.11	0.11	0.32	0.84	43
SST.mf	0.677	1.95	0.61	0.877	0.71	0.62	0.088	0.104	0.754	1.25	29
AFMSST.lf.3	0.0034	1.4	0.59	0.012	0.507	0.84	0.075	0.0828	0.31	1.0	10
AFMSST.mf.1	0.0805	1.03	0.32	0.25	0.69	0.71	0.075	0.0828	0.31	1.0	10
AFMSST.mf.2	0.0827	1.072	0.325	0.25	0.676	0.715	0.075	0.0828	0.31	1.0	10
AFMSST.lfmf.1	0.21	0.26	0.96	0.056	0.25	0.85	0.075	0.0828	0.71	0.91	9.53

SST.d = SST model with default coefficients
SST.lf = SST model with coefficient tuned to "lowFlow" case
SST.mf = SST model with coefficient tuned to "modFlow" case
$\gamma_d = 0.555556$

Fig. 7 shows the results of fitting exercise based on the "modFlow" case from Table 2. Once again, the standard SST model (SST.d) does not well represent the wall temperature along the heated section and exhibits strongly exaggerated features. An optimized SST model (SST.mf) is significantly better at representing the target data. The AFMSST.mf.X models with AFM transport equations was also tuned to the "modFlow" data and was able to represent the data moderately better than the optimized SST model. The AFM.lfmf.1 model is an improvement over the SST.d model but otherwise poorly represents the data qualitatively.

3.3.2 Model Testing and Discussion

Fig. 8 shows the results of testing models tuned to the "modFlow" case by simulating the "lowFlow" scenario. All models line up well with the left edge of local peaking. However, only AFMSST.lfmf.1, which was tuned to both cases, is able to capture the lower temperature after the peak. The default SST model (SST.d) and models tuned to only the "modFlow" data fail to represent key physics of the supercritical fluid. Comparing the AFM coefficients (Table 3) shows that the primary difference between AFMSST.mf.2 and AFMSST.lfmf.1 are the C_{t1} and SST transport equation coefficients, highlighting the importance of the temperature gradient and turbulent mixing. The c'_{t1} coefficient is also somewhat different, but SST is a linear model and the turbulence anisotropy tensor will not contribute. This term was included for completeness and the value produced is likely a fitting artifact. Once again, these results underscore the importance of coefficient set selection. The physics embedded in the "modFlow" models are shown here to be mostly unable to reproduce the physics of the "lowFlow" case without embedding the right physics through data fitting.

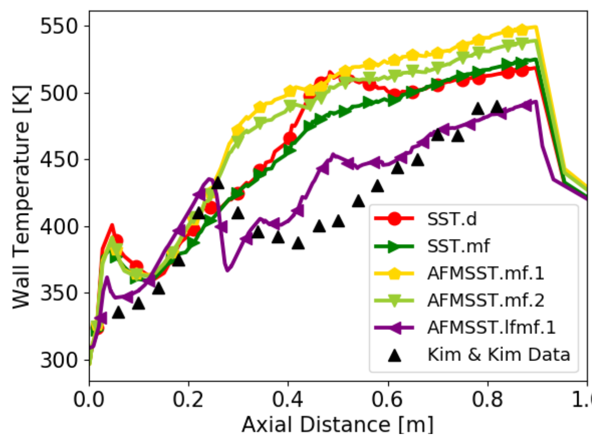

Figure 8: Testing of SST-based models on "lowFlow" case. SST.d is default *OpenFOAM* model. SST.mf, AFMSST.mf.1, AFMSST.mf.2, and AFMSST.lfmf.1 are models developed by Illinois Rocstar. Data from Kim and Kim [29].

Fig. 9 shows the results of testing models to the "lowFlow" case by simulating the "modFlow" scenario. The AFMSST.lf.3 model behaves smoothly but significantly underpredicts the wall temperature and misses all qualitative features of the data. The SST.lf model approximately captures the small peak towards the left of the plot but underpredicts the wall temperature throughout the remainder of the heated section. In this case, the best performing model is the SST model with standard coefficients. SST.d qualitatively captures the peak near the inlet of the heated section and captures wall temperature "on average," in that the calculated temperature remains near the measured temperature.

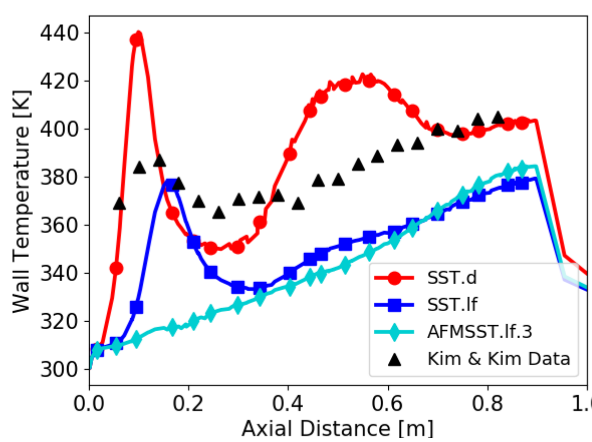

Figure 9: Testing of SST-based models on "modFlow" case. SST.d is default *OpenFOAM* model. SST.lf and AFMSST.lf.3 are models developed by Illinois Rocstar. Data from Kim and Kim [29].

The results suggest that the models tuned to one data set perform best within a flow rate regime. For example, the AFMSST.lf.3 model represents the "lowFlow" data especially well, shown in Fig. 6, but essentially fails to capture the temperature profile of the "modFlow" case, shown in Fig. 9. The same trend was exhibited by the cases tuned to the "modFlow" data. These observations motivated the creation of the AFMSST.lfmf.1 model, which was informed by both sets of data. While this model does not perfectly match either set of data, it outperforms the standard SST model as well as the other fitted models.

As further testing, radial profiles of the axial component of velocity were calculated. Fig. 10 shows these profiles just downstream of the beginning of the heated section. The “modFlow” case profiles appear to be essentially fully developed turbulent profiles. The maxima are at the center of the pipe and the velocity quickly vanishes near the wall. The “lowFlow” case exhibits a more interesting shape. The velocity peaks very near the wall in this case, showcasing the strong effects of buoyancy in this simulation. Fluid near the wall expands as heat is added, causing localized acceleration. At this location, all turbulence models produce similar velocity profiles. Fig. 11 shows velocity profiles near the center of the heated section. Substantial differences are readily noticeable in the flow profiles for both cases. All models show peaking near the wall boundaries consistent with buoyancy-driven acceleration. The SST.lf and AFMSST.lf.3 models show the least pronounced edge-peaking while SST.d shows the most pronounced. Fig. 12 shows velocity profiles just downstream of the outlet of the heated section. Most of the curves exhibit fully developed turbulent flow behavior.

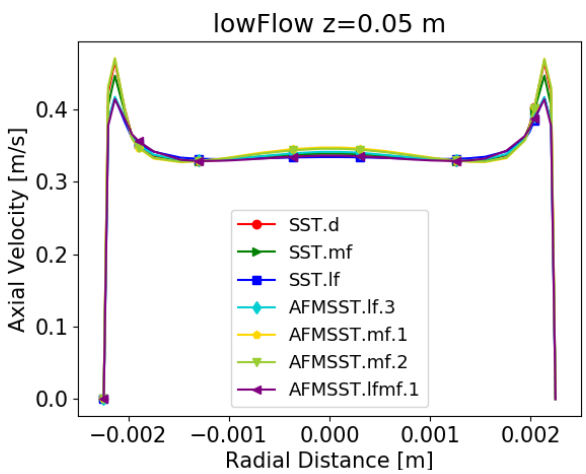

(a) “lowFlow” profiles.

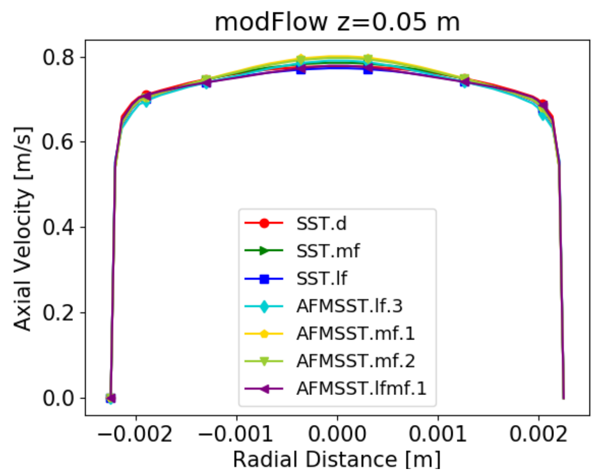

(b) “modFlow” profiles.

Figure 10: Velocity profiles for Kim and Kim cases just downstream of heated section inlet. SST.d is default *OpenFOAM* model. SST.mf, SST.lf, AFMSST.lf.3, AFMSST.mf.1, AFMSST.mf.2, and AFMSST.lfmf.1 are models developed by Illinois Rocstar.

Velocity profiles were not gathered by Kim and Kim [29] but the profiles presented here are in qualitative agreement with the results of Kurganov and Zeigarnik [40]. Supercritical flows in general are receiving a great deal of attention in the area of high accuracy simulations [41–43]. Comparisons to studies like these is left to future work and will provide valuable insight into flow phenomena.

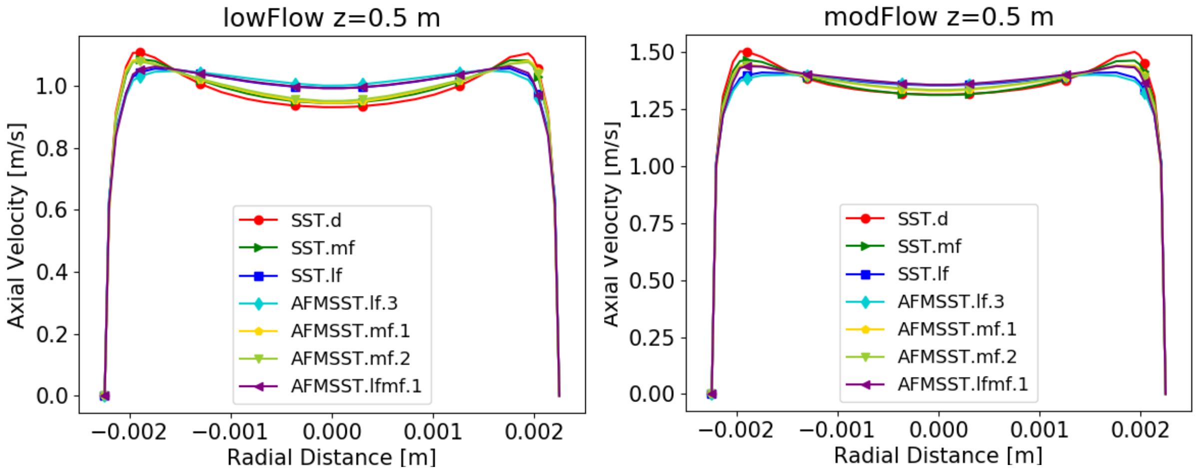

(a) “lowFlow” profiles. **(b)** “modFlow” profiles.

Figure 11: Velocity profiles for Kim and Kim cases near center of heated section. SST.d is default *OpenFOAM* model. SST.mf, SST.lf, AFMSST.lf.3, AFMSST.mf.1, AFMSST.mf.2, and AFMSST.lfmf.1 are models developed by Illinois Rocstar.

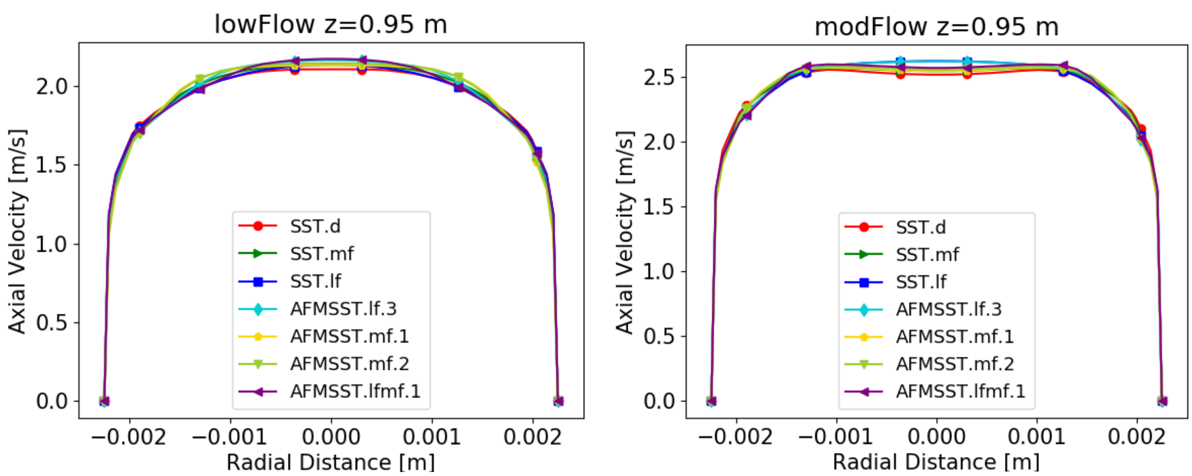

(a) “lowFlow” profiles. **(b)** “modFlow” profiles.

Figure 12: Velocity profiles for Kim and Kim cases just downstream of heated section outlet. SST.d is default *OpenFOAM* model. SST.mf, SST.lf, AFMSST.lf.3, AFMSST.mf.1, AFMSST.mf.2, and AFMSST.lfmf.1 are models developed by Illinois Rocstar.

The flow fields inside the heated pipe are shown in Fig. 13. The temperature and velocity fields for the “lowFlow” case are shown in Figs. 13a and 13b, respectively. Temperature is highest near the wall and does not quickly penetrate into the bulk flow. White horizontal bars on the velocity figure show the locations of the radial velocity plots and roughly indicate the extent of the heated section. The flow speed increases as heat addition causes flow expansion. This acceleration strongly affects flow profiles throughout the heated section. Familiar fully developed profile shapes are evident through inlet and outlet sections. The temperature and velocity fields for the “modFlow” case are shown in Figs. 13c and 13d, respectively, and exhibit similar behavior to the “lowFlow” case. However, the temperature peak for the “lowFlow” case is much higher due to heat transfer deterioration. Downstream of this peak, the bulk temperature rapidly increases for the “lowFlow” case as the higher temperature difference increases heat transfer.

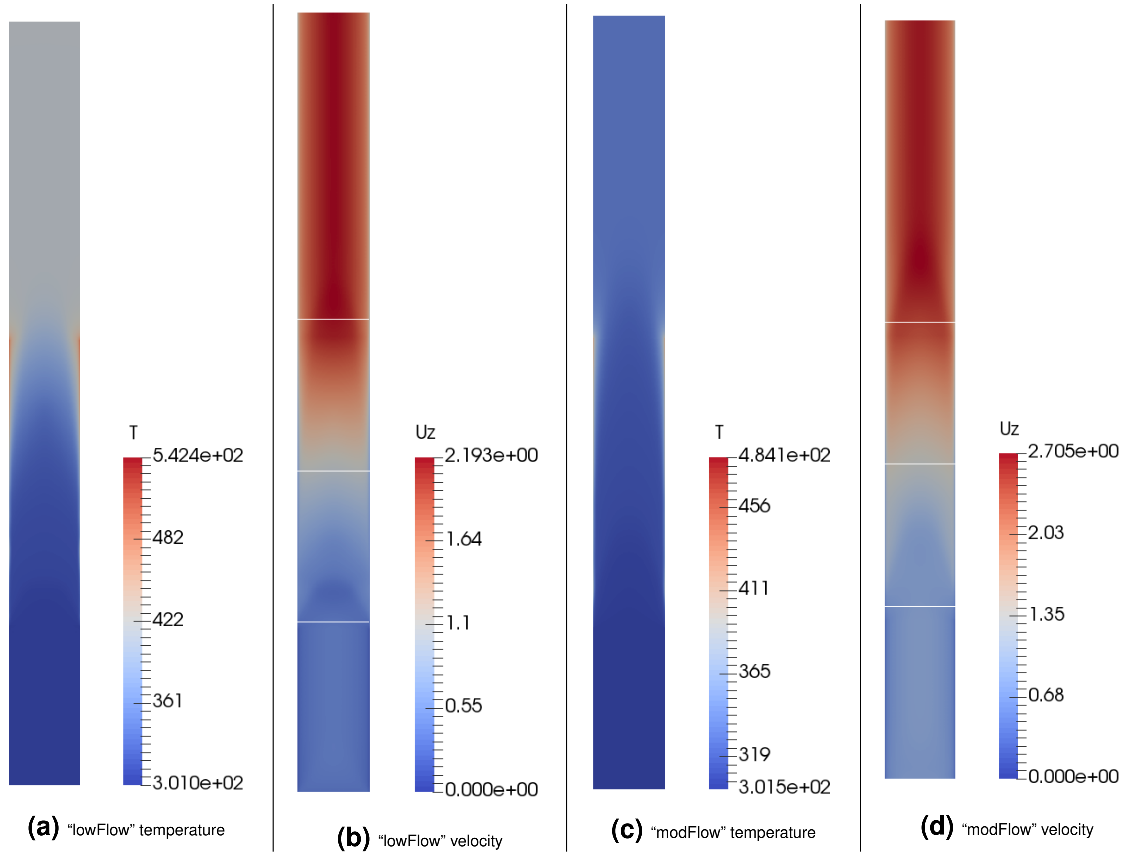

Figure 13: Temperature and velocity fields through the center plane of heated pipe. Axial direction shown at 1/50th scale. Horizontal white lines show locations from which radial velocity profiles were extracted. Inlet is located at bottom of the figure with outlet at the top.

3.4 Model Validation

As a validation case, the developed models were applied to the experiment performed by Zhang and colleagues [14]. This case is similar to that used for coefficient optimization (Section 3.2) in that the experiment is a heated pipe with supercritical fluid. However, as shown in Table 5, the validation case uses a different fluid and the system operating conditions (pressure, temperature) are substantially higher than the base cases. The differences are summarized in Table 6. To ensure that this study truly provided an assessment of predictiveness, the data published by Zhang et. al. were not used in developing any of the turbulence models with which they are being compared.

Table 5: Zhang test case parameters

Inlet Velocity [m/s]	Pressure [MPa]	Heat Flux [kW/m^2]	Inlet Temperature [°C]	fluid
2.873	25.0	1385	320	H_2O

A relatively fine mesh was used for the simulation with just over 1.3 million cell and $y^+ \approx 6$ from 5 layers of prismatic cells near the wall. Low Reynolds number wall functions were used for k and wall functions were used for ω. Wall functions for k_t and ω_t are as described in Section 2.4. This test case was treated as a "blind" benchmark (*i.e.* turbulence models were applied with best-guess parameters with no knowledge about the solution) and no efforts were made to improve

Table 6: Differences between tuning (Kim and Kim) and validation (Zhang) cases.

Case	Pressure [MPa]	Inlet Temperature [°C]	fluid
Kim and Kim	8.194-8.419	$\approx$ 29	CO_2
Zhang	25.0	320	H_2O

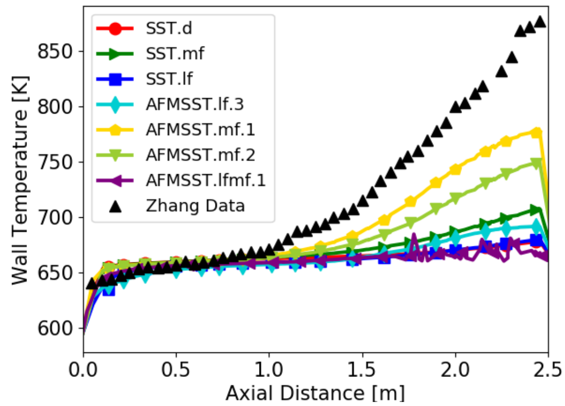

Figure 14: Comparison of SST-based models with experimental data as published by Zhang et al. [14]. SST.d is default *OpenFOAM* model. SST.mf, SST.lf, AFMSST.lf.3, AFMSST.mf.1, AFMSST.mf.2, and AFMSST.lfmf.1 are models developed by Illinois Rocstar.

wall treatment once results were gathered. We sought to only apply knowledge gained from the "modFlow" and "lowFlow" cases discussed above to assess the state of validation.

Fig. 14 shows the results of all the developed SST based models used to simulate the Zhang test case. The unoptimized SST turbulence model (SST.d) predicted the wall temperatures quite poorly. The SST model with coefficients tuned to the "modFlow" experiment (SST.mf) shows some qualitative improvement of the default and SST.lf models. The models that show the best quantitative performance are those tuned to the "modFlow" experiment. For this case AMFSST.mf.1 is the "best" performing model. The Zhang experiment chosen for validation features no local peaking as in the "lowFlow" Kim and Kim case and is therefore more directly related to the "modFlow" case.

The results from this validation study suggest that AMFSST.mf.1 is at least qualitatively predictive for heated supercritical channel flows without the occurrence of heat transfer. Testing under those conditions is left to future work. This result highlights the importance of using appropriate turbulence models for capturing supercritical phenomena. Even though SST.mf and AMFSST.mf.1 were tuned to the same data, the four equation model with AFM substantially outperformed the two equation SST model. The additional sensitivities provided by the algebraic flux assumption provide the framework to incorporate the complex turbulence and heat transfer effects of the strong variation of thermophysical properties with temperatures characteristic of supercritical fluids.

4 Conclusions and Future Work

We designed, implemented, and optimized a framework for the production of RANS turbulence models based on existing experimental data published in the scientific literature. This framework produced several novel four equation k_t-ω_t turbulence models based on SST RANS models along with the algebraic flux model for the buoyancy production term. We developed the models iteratively by tuning coefficients to published data from experimental programs conducted on heated tubes with forced sCO_2 flow. Optimized models with AFM transport equations were shown better able to represent complex phenomena such as heat transfer deterioration than standard RANS models without AFM. The predictive capacity of these models is presently uncertain and validation will be the subject of substantial future efforts. However, the AFMSST.mf.1 model exhibits predictive properties for supercritical fluids with moderate flow rates.

The model was shown to exhibit sensitivity to near wall mesh, especially the y^+ value. The limitations of the work presented here constrained us to wall-modeled approaches. Therefore, the reader should pay attention to the near-wall mesh when using this k_t-ω_t approach. Despite this sensitivity, the modeling approach represents a step forward for developing cost-effective models tailored to the challenges of supercritical flows. Extending this work to wall-resolved approaches is expected to substantially relax the constraints of the near wall mesh.

The turbulence model development carried out through this work is summarized in Fig. 15. As discussed in detail in Sections 2 and 3, this work uses pre-published experimental data from the scientific literature which primarily consists of forced flow through heated tubes. Fig. 15a illustrates the effects of fitting model coefficients to experimental data from Kim and Kim [29]. In this case, the standard shear stress transport (SST.d) model very poorly represents the wall temperature of the channel. However, the addition of the algebraic flux model and coefficient tuning allows the AFMSST.lf.3 model to much better represent the data, both qualitatively and quantitatively. Fig. 15b summarizes the efforts taken to assess the predictive capabilities of the developed RANS models. In this case, the models were used to simulate a scenario characterized by higher operating pressures and temperatures as well as a different working fluid (supercritical water vs. sCO_2). The Zhang data [14] were not used in model formulation. The best performing model (AFMSST.mf.1) represents a marked improvement over the SST.d model.

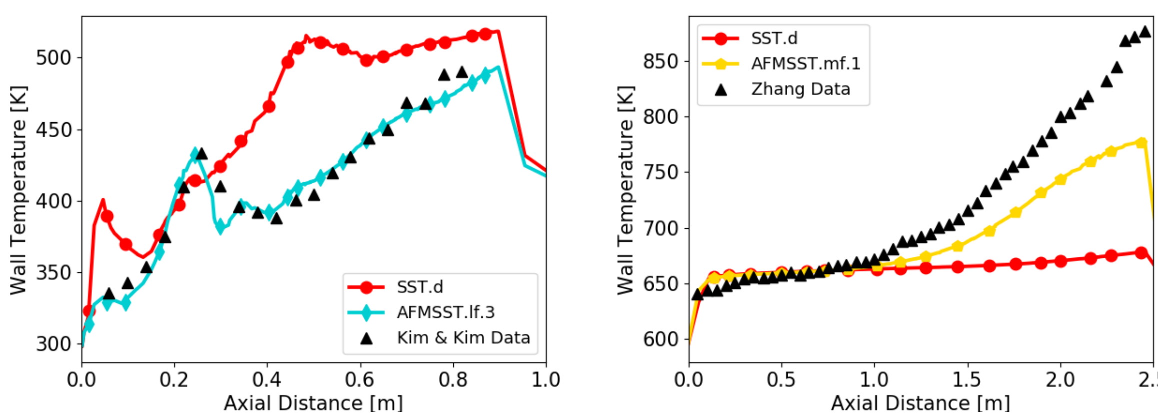

(a) Models were tuned by embedding experimental data in semi-empirical turbulence coefficients through non-linear optimization techniques.

(b) Model predictiveness was assessed through application to conditions well outside those used to tune the coefficient sets.

Figure 15: Tuning model coefficients (left) to match experimental data. SST.d is default model. AFMSST.lf.3 is model with coefficients tuned to data shown in black. To validate data (right), model predictions are compared to data which were not used in model formulation.

Future work will focus on expanding the data set to which the models are tuned with hopes of widening the range of applicability. For example, optimizing coefficient sets with both "lowFlow" and "modFlow" data is hoped to produce a predictive model with less restriction on system flow rate. Adding isothermal data will help ensure the model performs well in regions away from the critical point or high thermal gradients. Further, developing improved wall treatment formulations for future models will likely improve results. The treatment used here was based on existing formulations for the standard k and ω fields. More advanced wall functions may be constructed to include buoyant effects that can potentially increase the fidelity of these models [44–46] with sensitivity to anisotropic turbulence and streamline curvature added through nonlinear constitutive models. We anticipate that adding these into supercritical flow models will improve capabilities for highly complex flows such as those found in turbomachinery. Extending the present analysis to wall resolved meshes will be important in short term future work to more accurately capture near wall buoyancy effects.

The models created during this work were subject to several iterations of the fitting procedure, as indicated by the number at the end of each model name. Continued iteration on the lfmf model in the form of adjustments made to the starting set of coefficients or fitting subsets of coefficients separately is likely to improve the performance of the model. Further validation through comparisons to experimental data should be the subject of substantial future efforts. In general, the four equation AFM approach appears to be well-suited to the challenge of supercritical flow modeling and simulation and shows promise for assisting the supercritical fluid power cycles industry.

5 Acknowledgments

This material is based upon work supported by the U.S. Department of Energy, Office of Science, Small Business Innovation Research (SBIR) Program under Award Number(s) Grant No. DE-SC0017236. The author wishes to acknowledge Luke Calian for his efforts to enable table-based equations of state in *OpenFOAM* v4.1.

References

[1] IEA Publications, and International Energy Agency, “2017 World Energy Outlook,” OECD/IEA, Tech. Rep., Nov. 2017. [Online]. Available: https://www.iea.org/weo2017/

[2] R. Allam, S. Martin, B. Forrest, J. Fetvedt, X. Lu, D. Freed, G. W. Brown Jr, T. Sasaki, M. Itoh, and J. Manning, “Demonstration of the Allam Cycle: an update on the development status of a high efficiency supercritical carbon dioxide power process employing full carbon capture,” *Energy Procedia*, vol. 114, pp. 5948–5966, 2017.

[3] X. Cheng and X. Liu, “Research status and prospect of supercritical water-cooled reactor,” *Atomic Energy Science and Technology*, vol. 42, no. 2, pp. 167–172, 2008.

[4] U. S. Department of Energy, “Quadrennial Technology Review 2015 Chater 4: Advancing Clean Electric Power Technologies,” Tech. Rep., 2015. [Online]. Available: https://energy.gov/sites/prod/files/2016/06/f32/QTR2015-4R-Supercritical-Carbon-Dioxide-Brayton%20Cycle.pdf

[5] J. Tyacke, P. Tucker, R. Jefferson-Loveday, N. R. Vadlamani, R. Watson, I. Naqavi, and X. Yang, “Large eddy simulation for turbines: methodologies, cost and future outlooks,” *Journal of Turbomachinery*, vol. 136, no. 6, p. 061009, 2014.

[6] R. B. Duffey and I. L. Pioro, "Experimental heat transfer of supercritical carbon dioxide flowing inside channels (survey)," *Nuclear Engineering and Design*, vol. 235, no. 8, pp. 913–924, 2005.

[7] J. H. Bae, J. Y. Yoo, and H. Choi, "Direct numerical simulation of turbulent supercritical flows with heat transfer," *Physics of fluids*, vol. 17, no. 10, p. 105104, 2005.

[8] K. Xu, B. Ruan, and H. Meng, "Validation and analyses of RANS CFD models for turbulent heat transfer of hydrocarbon fuels at supercritical pressures," *International Journal of Thermal Sciences*, vol. 124, pp. 212–226, 2018.

[9] K. Abe, T. Kondoh, and Y. Nagano, "A new turbulence model for predicting fluid flow and heat transfer in separating and reattaching flowsI. Flow field calculations," *International journal of heat and mass transfer*, vol. 37, no. 1, pp. 139–151, 1994.

[10] ——, "A new turbulence model for predicting fluid flow and heat transfer in separating and reattaching flowsII. Thermal field calculations," *International Journal of Heat and Mass Transfer*, vol. 38, no. 8, pp. 1467–1481, 1995.

[11] C. B. Hwang and C. A. Lin, "A low Reynolds number two-equation $k_\theta - \tilde{\epsilon}_\theta$ model to predict thermal fields," *International journal of heat and mass transfer*, vol. 42, no. 17, pp. 3217–3230, 1999.

[12] B. Deng, W. Wu, and S. Xi, "A near-wall two-equation heat transfer model for wall turbulent flows," *International journal of heat and mass transfer*, vol. 44, no. 4, pp. 691–698, 2001.

[13] S. Kenjereš, S. B. Gunarjo, and K. Hanjalić, "Contribution to elliptic relaxation modelling of turbulent natural and mixed convection," *International Journal of Heat and Fluid Flow*, vol. 26, no. 4, pp. 569–586, 2005.

[14] G. Zhang, H. Zhang, H. Gu, Y. Yang, and X. Cheng, "Experimental and numerical investigation of turbulent convective heat transfer deterioration of supercritical water in vertical tube," *Nuclear Engineering and Design*, vol. 248, pp. 226–237, Jul. 2012. [Online]. Available: http://www.sciencedirect.com/science/article/pii/S0029549312001586

[15] Y.-Y. Bae, E.-S. Kim, and M. Kim, "Assessment of low-Reynolds number k- turbulence models against highly buoyant flows," *International Journal of Heat and Mass Transfer*, vol. 108, pp. 529–536, 2017.

[16] ——, "Numerical simulation of upward flowing supercritical fluids using buoyancy-influence-reflected turbulence model," *Nuclear Engineering and Design*, vol. 324, pp. 231–249, 2017.

[17] F. Ries, P. Obando, I. Shevchuck, J. Janicka, and A. Sadiki, "Numerical analysis of turbulent flow dynamics and heat transport in a round jet at supercritical conditions," *International Journal of Heat and Fluid Flow*, vol. 66, pp. 172–184, 2017.

[18] M. Sharabi, W. Ambrosini, S. He, and J. D. Jackson, "Prediction of turbulent convective heat transfer to a fluid at supercritical pressure in square and triangular channels," *Annals of Nuclear Energy*, vol. 35, no. 6, pp. 993–1005, 2008.

[19] M. Sharabi and W. Ambrosini, "Discussion of heat transfer phenomena in fluids at supercritical pressure with the aid of CFD models," *Annals of Nuclear Energy*, vol. 36, no. 1, pp. 60–71, 2009.

[20] M. Mucci, N. Forgione, S. He, W. Ambrosini, and J. D. Jackson, “Assessment of turbulence models in the simulation of heat transfer to water at supercritical pressure in the upward and downward flow,” Pisa, Italy, Jul. 2010.

[21] M. De Rosa, G. Guetta, W. Ambrosini, N. Forgione, S. He, and J. D. Jackson, “Lessons learned from the application of CFD models in the prediction of heat transfer to fluids at supercritical pressure,” in *5TH International Symposium on Supercritical Water Reactors (ISSCWR-5)*, 2011, pp. 13–16.

[22] S. K. Debrah, W. Ambrosini, M. De Rosa, and N. Forgione, “Analysis of heat transfer to supercritical carbon dioxide by the STAR-CCM+ CFD code,” in *29th UIT Heat Transfer Conference*, 2011.

[23] W. Ambrosini, N. Forgione, S. Badiali, J. D. Jackson, and M. Sharabi, “Capabilites of Two-Equation Low-Reynolds Number Turbulence Models in Predicting Heat Transfer to Fluids at Supercritical Pressure,” in *Proceedings of the 15th International Topical Meeting on Nuclear Reactor Thermalhydraulics (NURETH-15), Pisa, Italy*, 2013.

[24] A. Pucciarelli, I. Borroni, M. Sharabi, and W. Ambrosini, “Results of 4-equation turbulence models in the prediction of heat transfer to supercritical pressure fluids,” *Nuclear Engineering and Design*, vol. 281, pp. 5–14, 2015. [Online]. Available: http://www.sciencedirect.com/science/article/pii/S0029549314005809

[25] V. Papp, A. Pucciarelli, M. Sharabi, and W. Ambrosini, “Use of Algebraic Heat Flux Models to Improve Heat Transfer Predictions for Supercritical Pressure Fluids,” in *2016 24th International Conference on Nuclear Engineering*. American Society of Mechanical Engineers, 2016, pp. V004T10A012–V004T10A012.

[26] A. Pucciarelli, M. Sharabi, and W. Ambrosini, “Prediction of heat transfer to supercritical fluids by the use of Algebraic Heat Flux Models,” *Nuclear Engineering and Design*, vol. 297, pp. 257–266, 2016.

[27] A. Pucciarelli and W. Ambrosini, “On the effect of conjugate heat transfer on turbulence in supercritical fluids: Results from a LES application,” *Annals of Nuclear Energy*, vol. 111, pp. 340–346, 2018.

[28] Y. Nagano and C. Kim, “A two-equation model for heat transport in wall turbulent shear flows,” *Journal of heat transfer*, vol. 110, no. 3, pp. 583–589, 1988.

[29] D. E. Kim and M.-H. Kim, “Experimental investigation of heat transfer in vertical upward and downward supercritical CO2 flow in a circular tube,” *International Journal of Heat and Fluid Flow*, vol. 32, no. 1, pp. 176–191, 2011. [Online]. Available: http://www.sciencedirect.com/science/article/pii/S0142727X10001578

[30] E.W. Lemmon, M.O. McLinden, and D.G. Friend, “Thermophysical Properties of Fluid Systems,” in *NIST Chemistry WebBook, NIST Standard Reference Database Number 69*, Gaithersburg MD, 20899.

[31] F. R. Menter, “Two-equation eddy-viscosity turbulence models for engineering applications,” *AIAA journal*, vol. 32, no. 8, pp. 1598–1605, 1994. [Online]. Available: http://arc.aiaa.org/doi/abs/10.2514/3.12149

[32] F. Menter and T. Esch, "Elements of industrial heat transfer predictions," in *16th Brazilian Congress of Mechanical Engineering (COBEM)*, vol. 109, 2001.

[33] F. R. Menter, M. Kuntz, and R. Langtry, "Ten years of industrial experience with the SST turbulence model," *Turbulence, heat and mass transfer*, vol. 4, no. 1, pp. 625–632, 2003.

[34] A. Hellsten, "Some improvements in Menter's k-omega SST turbulence model," in *29th AIAA, Fluid Dynamics Conference*, 1998, p. 2554.

[35] S. V. Patankar and D. B. Spalding, "A calculation procedure for heat, mass and momentum transfer in three-dimensional parabolic flows," in *Numerical Prediction of Flow, Heat Transfer, Turbulence and Combustion*. Elsevier, 1983, pp. 54–73.

[36] B. Van Leer, "Towards the ultimate conservative difference scheme. IV. A new approach to numerical convection," *Journal of computational physics*, vol. 23, no. 3, pp. 276–299, 1977.

[37] Chris Greenshields, "OpenFOAM 5.0 Released," Jul. 2017. [Online]. Available: https://openfoam.org/release/5-0/

[38] M. A. Branch, T. F. Coleman, and Y. Li, "A subspace, interior, and conjugate gradient method for large-scale bound-constrained minimization problems," *SIAM Journal on Scientific Computing*, vol. 21, no. 1, pp. 1–23, 1999.

[39] The SciPy community, "scipy.optimize.least_squares," May 2018. [Online]. Available: https://docs.scipy.org/doc/scipy/reference/generated/scipy.optimize.least_squares.html

[40] V. A. Kurganov and Y. A. Zeigarnik, "Results of studying of turbulent heat transfer deterioration in channels and their application in practical calculations of heat transfer and pressure drop of supercritical pressure coolants," in *Proceedings of 11th International Topical Meeting on Nuclear Reactor Thermal Hydraulics (NURETH-11), Avignon, France, Oct*, 2005, pp. 2–6.

[41] J. W. R. Peeters, R. Pecnik, B. J. Boersma, T. van der Hagen, and M. Rohde, "Near Wall Structures in Turbulent Flows with Strong Thermo-Physical Property Variations," in *Direct and Large-Eddy Simulation X*. Springer, 2018, pp. 537–543.

[42] U. Sengupta, H. Nemati, B. J. Boersma, and R. Pecnik, "Fully compressible low-Mach number simulations of carbon-dioxide at supercritical pressures and trans-critical temperatures," *Flow, Turbulence and Combustion*, vol. 99, no. 3-4, pp. 909–931, 2017.

[43] S. Pandey, X. Chu, E. Laurien, and B. Weigand, "Buoyancy induced turbulence modulation in pipe flow at supercritical pressure under cooling conditions," *Physics of Fluids*, vol. 30, no. 6, p. 065105, 2018.

[44] W. Xu, Q. Chen, and F. T. M. Nieuwstadt, "A new turbulence model for near-wall natural convection," *International Journal of Heat and Mass Transfer*, vol. 41, no. 21, pp. 3161–3176, 1998.

[45] T. J. Craft, S. E. Gant, A. V. Gerasimov, H. Iacovides, and B. E. Launder, "Development and application of wall-function treatments for turbulent forced and mixed convection flows," *Fluid Dynamics Research*, vol. 38, no. 2, pp. 127–144, 2006.

[46] P. Kiš and H. Herwig, "The near wall physics and wall functions for turbulent natural convection," *International Journal of Heat and Mass Transfer*, vol. 55, no. 9, pp. 2625–2635, 2012.